Penultimate Effect in Ethylene–Styrene Copolymerization and the Discovery of Highly Active Ethylene–Styrene Catalysts with Increased Styrene Reactivity

ARTICLE *in* JOURNAL OF THE AMERICAN CHEMICAL SOCIETY · JULY 2007

Impact Factor: 12.11 · DOI: 10.1021/ja070061y · Source: PubMed

Article

Penultimate Effect in Ethylene–Styrene Copolymerization and the Discovery of Highly Active Ethylene–Styrene Catalysts with Increased Styrene Reactivity

Daniel J. Arriola, Marilyn Bokota, Richard E. Campbell,, Jerzy Klosin, Robert E. LaPointe, O. David Redwine, Ravi B. Shankar, Francis J. Timmers, and Khalil A. Abboud

J. Am. Chem. Soc., **2007**, 129 (22), 7065-7076 • DOI: 10.1021/ja070061y

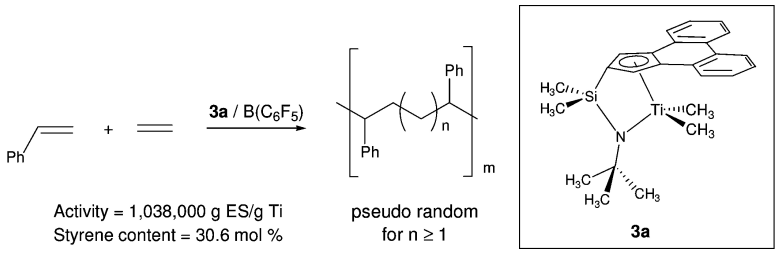

More About This Article

Additional resources and features associated with this article are available within the HTML version:

- Supporting Information
- Links to the 7 articles that cite this article, as of the time of this article download
- Access to high resolution figures
- Links to articles and content related to this article
- Copyright permission to reproduce figures and/or text from this article

View the Full Text HTML

J|A|C|S
ARTICLES
Published on Web 05/10/2007

Penultimate Effect in Ethylene−Styrene Copolymerization and the Discovery of Highly Active Ethylene−Styrene Catalysts with Increased Styrene Reactivity

Daniel J. Arriola,[†] Marilyn Bokota,[†] Richard E. Campbell, Jr.,[†] Jerzy Klosin,*[,†]
Robert E. LaPointe,[†] O. David Redwine,[†] Ravi B. Shankar,[†]
Francis J. Timmers,*[,†] and Khalil A. Abboud[‡]

Contribution from Corporate R&D, The Dow Chemical Company, 1776 Building, Midland, Michigan 48674, and Department of Chemistry, University of Florida, Gainesville, Florida 32611

Received January 4, 2007; Revised Manuscript Received March 21, 2007; E-mail: jklosin@dow.com; timmersfj@dow.com

Abstract: For the first time commercially relevant catalysts for the copolymerization of ethylene and styrene have been identified. The catalysts maintain very high copolymer efficiencies at relatively high reactor temperatures without sacrificing styrene comonomer reactivity. The observations which led to this discovery are based upon the kinetic analysis of ethylene−styrene copolymerization using constrained geometry catalyst (η^5-C_5Me_4)($SiMe_2$-N-*t*-Bu)$TiMe_2$ (**1**). This analysis revealed a substantial styrene penultimate monomer effect. Inherent reactivity of **1** toward styrene is greatly improved when the penultimate monomer on the growing polymer chain is styrene rather than ethylene. The presence of a penultimate styrene effect led to the hypothesis that catalysts bearing aromatic moieties in close proximity to the active site could lead to enhancement of styrene reactivity for this catalyst family. This hypothesis was born out by two new constrained geometry catalysts, one having two phenyl substituents placed in the 3 and 3′ positions of the Cp ring (**2**) and the other with a 2,2′-biphenyl fragment attached to the Cp ring (**3**). Both catalysts exhibit higher activity than that of **1** and, more importantly, much higher styrene reactivity leading to copolymers with substantially increased styrene content (21.5% for **2**, 30.6% for **3**) as compared to **1** (11%) under the same polymerization conditions. Analysis of the X-ray crystal structures of **2** and **3** shows no overriding structural arguments for the increased performance. Outstanding polymerization characteristics achieved with **3** make this catalyst a candidate for commercial production of ethylene−styrene resins in a solution process.

Introduction

Ethylene−styrene (ES) copolymers display a unique set of physical characteristics that fill property gaps not addressed by their respective polymer families, polyethylene and polystyrene, or by blends of these polymer families.[1] The polymers range from crystalline to amorphous depending upon co-styrene content. The copolymers accept large quantities of fillers without a substantial sacrifice in performance. As new materials, they offer unique opportunities to explore or expand new markets and to broaden basic polymer chemistry knowledge.

Despite the fact that styrene and ethylene are two of the most commercially important olefinic monomers, leading to the ubiquitous polymer families of polystyrene and polyethylene, respectively, a commercial offering of a random copolymer of these two monomers remains elusive. Strategies for producing ES copolymers which rely upon introducing the unconventional monomer into a conventional process (i.e., radical, Ziegler−Natta) invariably lead to homopolymer blends and copolymers with very low levels of the unconventional monomer.

In the early development of constrained geometry catalysts (CGC), copolymerization of ethylene with a variety of α-olefins was investigated. In addition to outstanding ethylene/octene copolymerization characteristics, (η^5-C_5Me_4)($SiMe_2$-N-*t*-Bu)$TiMe_2$ (**1**) and its analogues were also unexpectedly found to be very effective in copolymerizing ethylene and styrene producing pseudo-random ES copolymers.[2] Excellent performance of **1** for ES copolymerization was a significant breakthrough as this was the first time that a high activity, single-site,[3] ES catalyst which yields high molecular weight polymers had been identified. Since our initial discovery a significant amount of research has been devoted to ES polymerization using various CGC complexes.[4] Other catalytic systems have also been investigated for ES polymerization,[5] including mono-Cp titanium complexes,[4h,i,6]

[†] The Dow Chemical Company.
[‡] University of Florida.

(1) (a) Cheung, Y. W.; Guest, M. J. In *Modern Styrenic Polymers: Polystyrenes and Styrenic Copolymers*; Scheirs, J., Priddy, D. B., Eds.; John Wiley & Sons Ltd.: 2003; pp 605−630. (b) Guest, M. J.; Cheung, Y. W.; Diehl, C. F.; Hoenig, S. M. In *Metallocene-Based Polyolefins*; Scheirs, J., Kaminsky, W., Eds.; John Wiley & Sons Ltd.: 2000; Vol. 2, pp 271−292.

(2) (a) Stevens, J. C.; Timmers, F. J.; Wilson, D. R.; Schmidt, G. F.; Nickias, P. N.; Rosen, R. K.; Knight, G. W.; Lai, S. Eur. Patent 416815, 1991 (The Dow Chemical Company). (b) Timmers, F. J. U.S. Patent 6,670,432 B1, 2003 (The Dow Chemical Company).

(3) Previously investigated catalysts based on mono-Cp-TiX_3 produced, in addition to ES polymers, substantial amounts of polyethylene and polystyrene homopolymer impurities.

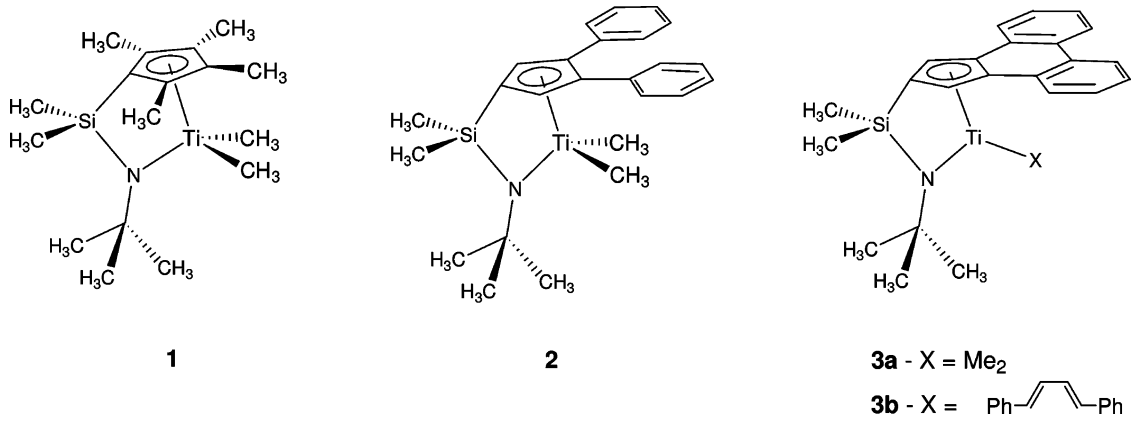

Figure 1. Constrained geometry procatalysts used in this study.

bis-Cp(indenyl) complexes,[4e,7] and non-Cp complexes.[8] Several computational papers on the ES polymerization mechanism have also been recently published.[9] Exploration of various metallocene-based catalysts for ES copolymerization within the past 15 years has led to the synthesis of ES polymers with different styrene distributions and stereochemistry along the polymer backbone. In addition to random ES copolymers, alternating ethylene/styrene,[6c] stereoregular ethylene/styrene,[4e,6g,7c] block ethylene/styrene,[7d,h] and ethylene/syndiotactic polystyrene[6l] have been reported. Living ES copolymerization has been recently reported as well.[6m] Of the ES copolymers prepared to date, random ES copolymers represent the best option for commercial production. The requirements for commercially relevant ES catalysts are very rigorous and include the following: (a) high catalytic activity (>1000 kg of ES/g of catalyst), (b) ability to operate at high reactor temperatures (>120 °C), (c) high molecular weight capabilities (>Mw of 100 K) at high reactor temperature, (d) high reactivity toward styrene, and (e) single site behavior (absence of ethylene or styrene homopolymer formation). The first two desired catalyst attributes are necessary from the perspective of process economics as well as polymer quality, since low catalytic activities lead to resins containing unacceptable levels of catalyst residue which might result in polymer discoloration and a decrease of physical properties. High reactivity toward styrene is of critical importance as it allows maintaining low styrene concentration in the reactor, which in turn minimizes formation of atactic polystyrene (aPS) resulting from thermal polymerization of this self-polymerizing monomer. Furthermore, lower concentrations of styrene minimize the demands of the post-polymerization styrene monomer recovery steps. While ES polymers with very high levels of co-styrene (approaching 50 mol %) can be prepared using **1**, the polymerization conditions are forced (i.e., neat styrene with low ethylene concentration) and are not conducive to commercial operations. We, therefore, sought to improve substantially upon the catalytic performance of **1** for the economical production of ethylene−styrene resins. In this paper, we present the results of the kinetic analyses of **1** in ES copolymerization, which led to the design of two new catalysts, **2** and **3** (Figure 1),[10] which exhibit substantially higher copolymerization activity and styrene reactivity compared to **1**.

(4) (a) Sernetz, F. G.; Mülhaupt, R. *Macromol. Chem. Phys.* **1996**, *197*, 1071−1083. (b) Sernetz, F. G.; Mülhaupt, R.; Amor, F.; Eberle, T.; Okuda, J. *J. Polym. Sci., Part A: Polym. Chem.* **1997**, *35*, 1571−1578. (c) McAdon, M. H.; Nickias, P. N.; Patton, J. T.; Shankar, R. B.; Timmers, F. J.; Vanderlende, D. D.; Kolthammer, B. W.; Ueligger, S.; Steven, M. U.S. Patent 5,965,756, 1999, (The Dow Chemical Company). (d) Xu, G. *Macromolecules* **1998**, *31*, 2395−2402. (e) Arai, T.; Ohtsu, T.; Suzuki, S. *Macromol. Rapid Commun.* **1998**, *19*, 327−331. (f) Sukhova, T. A.; Panin, A. N.; Babkina, O. N.; Bravaya, N. M. *J. Polym. Sci., Part A: Polym. Chem.* **1999**, *37*, 1083−1093. (g) Xu, G.; Cheng, D. *Polym. Prepr. (Am. Chem. Soc. Div. Polym. Chem.*) **2001**, *42*, 474−475. (h) Nomura, K.; Okumura, H.; Komatsu, T.; Naga, N.; Imanishi, Y. *J. Mol. Catal. A: Chem.* **2002**, *190*, 225−234. (i) Nomura, K.; Okumura, H.; Komatsu, T.; Naga, N. *Macromolecules* **2002**, *35*, 5388−5395. (j) Noh, S. K.; Yang, Y.; Lyoo, W. S. *J. Appl. Polym. Sci.* **2003**, *90*, 2469−2474. (k) Skeřil, R.; Šindelář, P.; Salajka, Z.; Varga, V.; Císařová, I.; Pinkas, J.; Horáček, M.; Mach, K. *J. Mol. Catal. A: Chem.* **2004**, *224*, 97−103. (l) Noh, S. K.; Lee, M.; Kum, D. H.; Kim, K.; Lyoo, W. S.; Lee, D-H. *J. Polym. Sci., Part A: Polym. Chem.* **2004**, *42*, 1712−1723. (m) Gentil, S.; Pirio, N.; Meunier, P.; Gallou, F.; Paquette, L. A. *Eur. Polym. J.* **2004**, *40*, 2241−2246. (n) Guo, N.; Li, L.; Marks, T. J. *J. Am. Chem. Soc.* **2004**, *126*, 6542−6543. (o) Martínez, S.; Exposito, M. T.; Ramos, J.; Cruz, V.; Martínez, M. C.; López, M.; Muñoz-Escalona, A.; Martínez-Salazor, J. *J. Polym. Sci., Part A: Polym. Chem.* **2005**, *43*, 711−725.

(5) For a review on ethylene−styrene polymerization, see: Pellecchia, C.; Oliva, L. *Rubber Chem. Technol.* **1999**, *72*, 553−558.

(6) (a) Longo, P.; Grassi, A.; Oliva, L. *Makromol. Chem.* **1990**, *191*, 2387−2396. (b) Aaltonen, P.; Seppälä, J. *Eur. Polym. J.* **1994**, *30*, 683−687. (c) Pellecchia, C.; Pappalardo, D.; D'Arco, M.; Zambelli, A. *Macromolecules* **1996**, *29*, 1158−1162. (d) Oliva, L.; Mazza, S.; Longo, P. *Macromol. Chem. Phys.* **1996**, *197*, 3115−3122. (e) Xu, G.; Lin, S. *Macromolecules* **1997**, *30*, 685−693. (f) Wu, Q.; Ye, Z.; Gao, Q.; Lin, S. *Macromol. Chem. Phys.* **1998**, *199*, 1715−1720. (g) Venditto, V.; De Tullio, G.; Izzo, L.; Oliva, L. *Macromolecules* **1998**, *31*, 4027−4029. (h) Pellecchia, C.; Pappalardo, D.; Oliva, L.; Mazzeo, M.; Gruter, G.-J. *Macromolecules* **2000**, *33*, 2807−2814. (i) Gentil, S.; Pirio, N.; Meunier, P.; Gallou, F.; Paquette, L. A. *Eur. Polym. J.* **2004**, *40*, 2241−2246. (j) Ishiyama, T.; Miyoshi, K.; Nakazawa, H. *J. Mol. Catal. A: Chem.* **2004**, *221*, 41−45. (k) Yokota, K.; Kohsaka, T.; Ito, K.; Ishihara, N. *J. Polym. Sci. Part A: Polym. Chem.* **2005**, *43*, 5041−5048. (l) Luo, Y.; Baldamus, J.; Hou, Z. *J. Am. Chem. Soc.* **2004**, *126*, 13910−13911. (m) Zhang, H.; Nomura, K.; *J. Am. Chem. Soc.* **2005**, *127*, 9364−9365.

(7) (a) Oliva, L.; Caporaso, L.; Pellecchia, C.; Zambelli, A. *Macromolecules* **1995**, *28*, 4665−4667. (b) Oliva, L.; Longo, P.; Izzo, L.; Di, Serio, M. *Macromolecules* **1997**, *30*, 5616−5619. (c) Arai, T.; Ohlsu, T.; Suzuki, S. *Polym. Prepr. (Am. Chem. Soc. Div. Polym. Chem.*) **1998**, *39*, 422. (d) Hou, Z.; Tezuka, H.; Zhang, Y.; Yamazaki, H.; Wakatsuki, Y. *Macromolecules* **1998**, *31*, 8650−8652. (e) Izzo, L.; Oliva, L.; Proto, A.; Trofa, M. *Macromol. Chem. Phys.* **1999**, *200*, 1086−1088. (f) Albers, I.; Kaminsky, W.; Weingarten, U.; Werner, R. *Catal. Commun.* **2002**, *3*, 105−112. (g) Arai, T.; Hanasato, S.; Nakajima, M.; Ohtsu, T. *Polym. Prepr. (Am. Chem. Soc. Div. Polym. Chem.*) **2002**, *43*, 293. (h) Caporaso, L.; Izzo, L.; Sisti, I.; Oliva, L. *Macromolecules* **2002**, *35*, 4866−4870. (i) Exposito, M. T.; Martínez, S.; Ramos, J.; Cruz, V.; Lopez, M.; Muñoz-Escalona, A.; Haider, N.; Martinez-Salazar, J. *Polymer* **2004**, *45*, 9029−9038.

(8) (a) Fokken, S.; Spaniol, T. P.; Okuda, J.; Sernetz, F. G.; Mulhaupt, R. *Organometallics* **1997**, *16*, 4240−4242. (b) Sernetz, F. G.; Mulhaupt, R.; Fokken, S.; Okuda, J. *Macromolecules* **1997**, *30*, 1562−1569.

(9) (a) Muñoz-Escalona, A.; Cruz, V.; Mena, N.; Martínez, S.; Martinez-Salazar, J. *Polymer* **2002**, *43*, 7017−7026. (b) Martínez, S.; Cruz, V.; Muñoz-Escalona, A.; Martinez-Salazar, J. *Polymer* **2003**, *44*, 295−306. (c) Yang, S. H.; Jo, W. H.; Noh, S. K. *J. Chem. Phys.* **2003**, *119*, 1824−1837. (d) Ramos, J.; Munoz-Escalona, A.; Martinez, S.; Martinez-Salazar, J. *J. Chem. Phys.* **2005**, *122*, 074901/1−079401/4.

(10) (a) Campbell, R. E., Jr.; Timmers, F. J.; Shankar, R. B.; Arriola, D. J. U.S. Patent 6,150,297, 2000 (The Dow Chemical Company). (b) Klosin, J.; Feng, S. S.; Shankar, R. B.; Timmers, F. J. U.S. Patent 6,825,147, 2004 (The Dow Chemical Company).

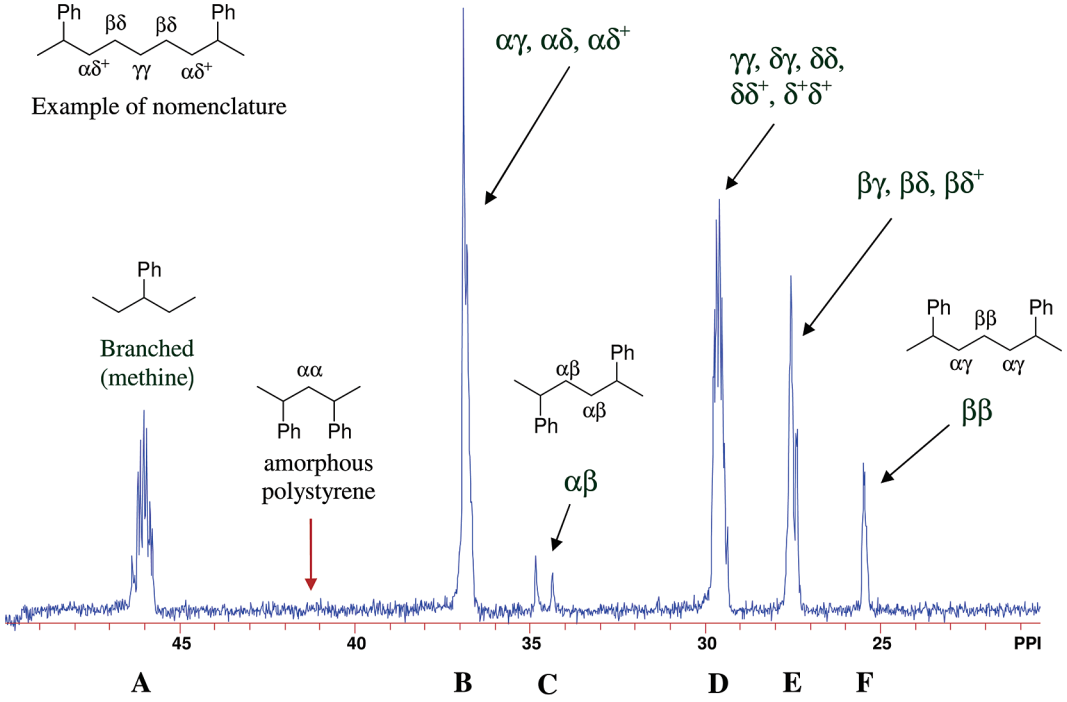

Figure 2. $^{13}C\{^1H\}$ NMR spectrum of an ES containing 31 mol % co-styrene using catalyst **3b**.

Results and Discussion

Ethylene−Styrene Copolymer Characterization. Conspicuous in the $^{13}C\{^1H\}$ NMR spectra of ES copolymers prepared using catalysts reported herein is the absence of signals due to isolated methylene units, designated αα methylenes, such as those observed in polystyrene (Figure 2).[11] This absence clearly indicates the catalyst's inability to insert two adjacent styrene monomers in a head-to-tail fashion. As a result, the upper limit of co-styrene in these ES copolymers is about 50 mol %. The spectrum[12] also reveals peaks attributed to isolated adjacent pairs of methylene units (αβ). The presence of these αβ methylene carbons indicates that styrene undergoes both [1,2] and [2,1] insertions, designated S_{12} (normal styrene insertion) and S_{21} (inverse styrene insertion), respectively.[13] However, it is not known whether the αβ methylene carbons arise from an $S_{12}-S_{21}$ or an $S_{21}-E-S_{12}$ sequence, or from both types of these insertion sequences. The two possibilities are shown below:

S_{12} followed by S_{21} S_{21} followed by E and then S_{12}

Regardless of how this microstructure forms, the presence of αβ methylene units is unequivocal evidence that styrene inserts in both a 1,2- and a 2,1-fashion since either sequence involves both types of styrene insertion modes. The overall population of sequences describes a unique monomer distribution in ES which we termed[2] pseudo-random, Scheme 1. Pseudo-random ES polymers are defined as polymers without sequential head-to-tail comonomer insertions and with a monomer distribution that is otherwise random or nearly so. This leads to sequences in the copolymers with two or more methylene units inserted between two methine units. Because the αβ-signal only arises when the S_{12} and S_{21} insertions are in very close proximity, inverse insertion is only observed at higher levels of co-styrene as isolated inverse styrene moieties in the polymer are indistinguishable from isolated normal styrene insertions.

Scheme 1. Monomer Addition Reactions Observed for Pseudo-random ES Copolymerization[a]

Allowed Addition Reactions

k_{p11}	Ti-E-P	+ **E**	→	Ti-**E**-E-P	ethylene addition
k_{p12}	Ti-E-P	+ $\mathbf{S_{12}}$	→	Ti-$\mathbf{S_{12}}$-E-P	normal styrene addition
k_{p13}	Ti-E-P	+ $\mathbf{S_{21}}$	→	Ti-$\mathbf{S_{21}}$-E-P	inverse styrene addition
k_{p21}	Ti-S_{12}-P	+ **E**	→	Ti-**E**-S_{12}-P	
k_{p23}	Ti-S_{12}-P	+ $\mathbf{S_{21}}$	→	Ti-$\mathbf{S_{21}}$-S_{12}-P	
k_{p31}	Ti-S_{21}-P	+ **E**	→	Ti-**E**-S_{21}-P	

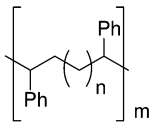

pseudo random for n ≥ 1

Unobserved (excluded) Addition Reactions

k_{p22}	Ti-S_{12}-P	+ $\mathbf{S_{12}}$	→	Ti-$\mathbf{S_{12}}$-S_{12}-P
k_{p32}	Ti-S_{21}-P	+ $\mathbf{S_{12}}$	→	Ti-$\mathbf{S_{12}}$-S_{21}-P
k_{p33}	Ti-S_{21}-P	+ $\mathbf{S_{21}}$	→	Ti-$\mathbf{S_{21}}$-S_{21}-P

[a] E, S_{12}, and S_{21} stand for ethylene (1), normal styrene (2), and inverse styrene (3), respectively; k_{pij} are the propagation rate constants of monomer j after an inserted i; and P represents the growing polymer chain.

The monomer copropagation rate equations are shown in Scheme 1. At the present time it is not known what the main styrene insertion mode is during ES polymerization with **1**. For the purposes of this discussion the predominant styrene insertion

(11) The convention used for assigning carbon methylene labels such as αβ describes the position relative to the nearest methine carbon in both directions along the polymer chain. Randall, J. C. *Rev. Macromol. Chem. Phys.* **1989**, *C29*, 201−317.

(12) The substituent effect parameter and corrective terms were taken from ref 11. The values for a phenyl substituent were obtained from: Pretsch, E.; Clerc, T.; Seible, J.; Simon, W. *Tables of Spectral Data for Structure Determination of Organic Compounds*; Springer-Verlag: 1989.

(13) A pair of αβ peaks of equal intensity arises from the relative stereochemical arrangement (*rac* and *meso*) of the phenyl substituents on either side of αβ methylene units.

mode is taken as [1,2] addition (S_{12}, normal styrene insertion), whereas the minor insertion mode is taken as [2,1] addition (S_{21}, inverse styrene insertion). However, the opposite assumption would yield the identical kinetic modeling result.

Steady-State Kinetic Modeling of 1 for ES. To gain a better understanding of the ES polymerization performance of catalyst **1**, a range of polymerization information was collected so that a kinetic model for the ES copolymerization process could be determined. The homogeneous polymerization media allowed for the use of the standard modeling equations for a continuous stirred-tank reactor (CSTR). Conversions were determined from monomer concentrations measured in real time. Using conversion as well as feed composition as inputs allowed for a direct prediction, of not only polymer composition but also comonomer distribution from dimensionless reactivity ratio parameters which are defined as follows (inverse styrene (S_{21}) is treated as a third monomer):

$$r_{12} = \left(\frac{k_{p11}}{k_{p12}}\right) \qquad r_{13} = \left(\frac{k_{p11}}{k_{p13}}\right) \qquad R = \left(\frac{k_{p23}}{k_{p21}}\right)$$

The concentration independent reactivity ratio r_{12} is the only parameter that would be required if this system had no reverse insertion and is a direct measure of the *inherent* reactivity of a given catalyst to a given pair of comonomers. Parameters r_{13} and the nonconventional reactivity ratio, R, are used to account for inverse styrene insertion in the copolymer which is only reflected in the $\alpha\beta$ methylene ^{13}C NMR signals. R is used to fit the $S_{12}-S_{21}$ sequence and r_{13} to fit the $S_{21}-E-S_{12}$ event. The polymerization experiments for this study were conducted over a temperature range from 50 to 90 °C, and the resulting ES samples spanned a composition range from 10 to nearly 38 mol % co-styrene (30−70 wt %). Frequently, r_{12} is very temperature dependent, and this value should be accompanied by the temperature to which it is referring. It has been our practice to compare 70 °C values.

The data was initially fitted to a first-order Markovian model consistent with Scheme 1 (i.e., a simple model), which resulted in a rather poor fit (*vide supra*) especially at high co-styrene compositions. Scheme 2 gives the reactivity ratio parameters and Arrhenius equation, and Figure 3 shows the first-order Arrhenius plot for complex **1** at 70 °C.

Scheme 2. Kinetic Parameters for **1** (70 °C) Using First-Order Markovian (Simple) Kinetic Model

$$r_{12}^{70^\circ} = 23.0 \qquad r_{12} = 23.0 \exp\left[\frac{-5462}{1.987}\left(\frac{1}{T} - \frac{1}{343\ K}\right)\right]$$

$$R^{70^\circ} = 0.020 \qquad E_{12} = 5462\ \text{cal/mol}$$

The value of the r_{13} reactivity ratio is not given because it approaches infinity and therefore has no impact on the model fit for catalyst **1** regardless of polymer composition or polymerization temperature. This kinetic result therefore suggests that the sequence that gives rise to the $\alpha\beta$ methylene signal is predominantly from the $S_{12}-S_{21}$ rather than the $S_{21}-E-S_{12}$ sequence.

Error analysis of this model indicates that the fit is composition dependent and begins to fail in predicting the clustering of co-styrene (SES sequence) in the ES polymers. Graph A in Figure 4 presents the measured versus the model predicted

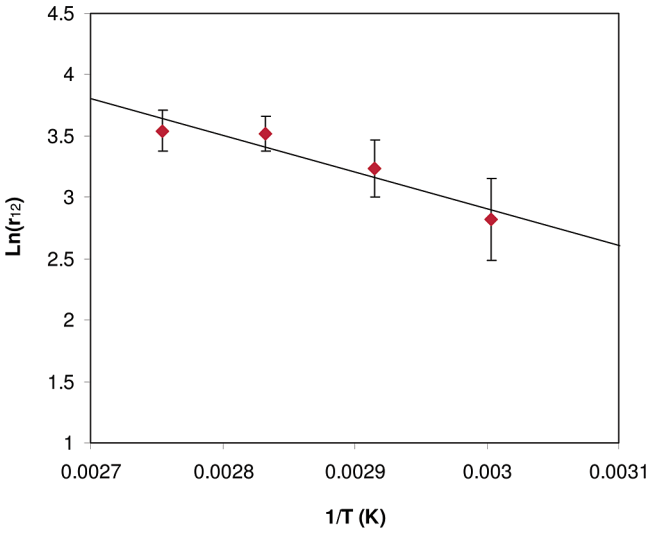

Figure 3. Arrhenius plot for **1** using the first-order Markovian kinetic model.

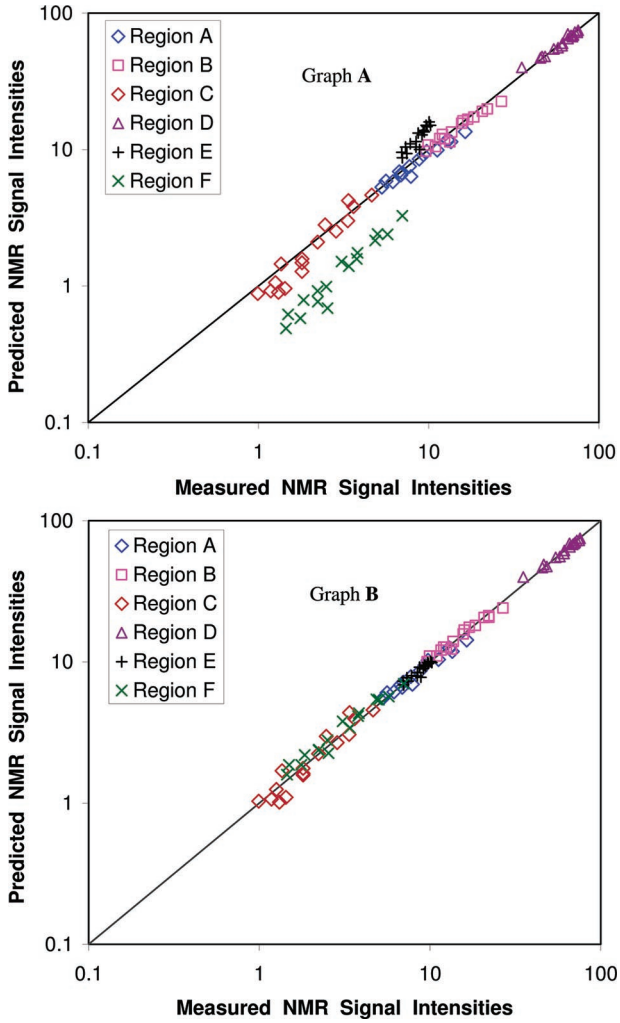

Figure 4. Observed versus predicted ^{13}C NMR signal intensities. (A) First-order Markovian model for catalyst **1**. (B) Second-order Markovian model for catalyst **1**.

signal intensities for each of the five regions in the ^{13}C NMR spectra for all the ES samples prepared with **1**. The fit is particularly poor for peaks in region F which are due to the $\beta\beta$ methylene in an SES triad. This observation suggests that this

Scheme 3. Penultimate Monomer Addition Reactions for ES Copolymerization

k_{p111}	Ti-E-E-P	+	**E**	→	Ti-**E**-E-E-P
k_{p211}	Ti-E-S_{12}-P	+	**E**	→	Ti-**E**-E-S_{12}-P
k_{p311}	Ti-E-S_{21}-P	+	**E**	→	Ti-**E**-E-S_{21}-P
k_{p112}	Ti-E-E-P	+	$\mathbf{S_{12}}$	→	Ti-$\mathbf{S_{12}}$-E-E-P
k_{p212}	Ti-E-S_{12}-P	+	$\mathbf{S_{12}}$	→	Ti-$\mathbf{S_{12}}$-E-S_{12}-P
k_{p312}	Ti-E-S_{21}-P	+	$\mathbf{S_{12}}$	→	Ti- $\mathbf{S_{12}}$-E-S_{21}-P
k_{p121}	Ti-S_{12}-E-P	+	**E**	→	Ti-**E**-S_{12}-E-P
k_{p123}	Ti-S_{12}-E-P	+	$\mathbf{S_{21}}$	→	Ti-$\mathbf{S_{21}}$-S_{12}-E-P
k_{p231}	Ti-S_{21}-S_{12}-P	+	**E**	→	Ti-**E**-S_{21}-S_{12}-P

simple kinetic model (above) does not reflect the complete catalytic character of **1** and that a second-order Markovian (penultimate) kinetic model for **1** should be considered to fully describe its kinetic behavior. Scheme 3 shows the monomer copropagation rate equations, k_{phij} (penultimate monomer h and ultimate monomer i attached to active metal reacting with free monomer, j). Effectively, the simple reactivity ratio, r_{12}, is the weighted average of three penultimate reactivity ratios.

The penultimate model was found to fit the ES ^{13}C NMR integrated areas across the composition range much better than the simple model for catalyst **1**. Graph B in Figure 4 shows a much improved fit for the observed versus predicted ^{13}C NMR signals for all peak areas compared to the fit obtained with the first-order Markovian model (graph A).

Scheme 4 shows the reactivity parameters at 70 °C and Arrhenius equations for the penultimate ES kinetic model for **1**; the Arrhenius plot for the reactivity ratios is shown in Figure 5. Note that E_{112} and E_{212} were allowed to be the same for this model. When E_{112} and E_{212} were allowed to vary independently, the model fit was not improved.

Scheme 4. Kinetic Parameters for **1** (70 °C) Using Second-Order Markovian (Penultimate) Kinetic Model

$$r_{112}^{70°} = \frac{k_{p111}}{k_{p112}} = 31.4 \qquad r_{112} = 31.4\exp\left[\frac{-3959}{1.987}\left(\frac{1}{T} - \frac{1}{343\ K}\right)\right]$$

$$r_{212}^{70°} = \frac{k_{p211}}{k_{p212}} = 6.47 \qquad r_{212} = 6.47\exp\left[\frac{-3959}{1.987}\left(\frac{1}{T} - \frac{1}{343\ K}\right)\right]$$

$$r_{312}^{70°} = \frac{k_{p311}}{k_{p312}} = 0.155 \qquad E_{112} = E_{212} = 3959\ \text{cal/mol}$$

$$R^{70°} = \frac{k_{p23}}{k_{p21}} = 0.013$$

Examination of the penultimate model kinetic parameters of **1** reveals a surprising trend, namely that *the inherent reactivity of the catalyst toward styrene is greatly improved when the penultimate monomer on the growing polymer chain is styrene rather than ethylene*. Furthermore, if one assumes that a normal mode of styrene insertion is [1,2] and inverse styrene is a [2,1] addition,[14] then, as the nearest pendant phenyl group on the growing polymer chain gets closer to the active metal center, the catalyst reactivity toward styrene monomers becomes greater

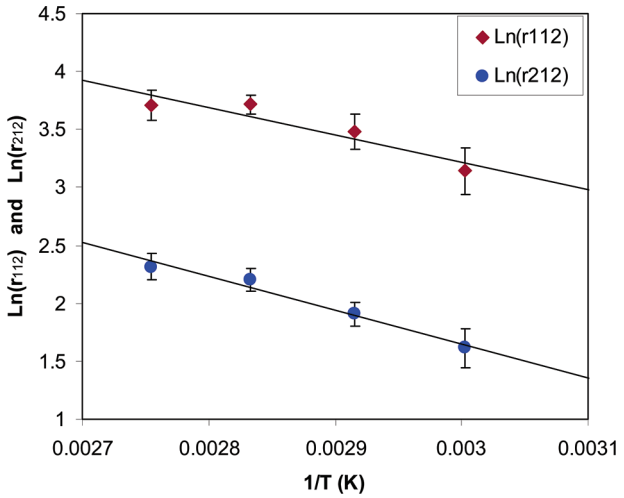

Figure 5. Arrhenius plot for **1** using the second-order Markovian kinetic model.

(compare r_{212} of 6.47 to r_{312} of 0.15). Although a rare event, it is remarkable that r_{312} is a value less than 1 which indicates that this catalyst species is inherently more reactive toward styrene than ethylene when the penultimate monomer is 2,1-inserted styrene despite increased steric congestion at the active site! The influence of a pendent phenyl side chain near the active site is not well understood, but if the phenomenon has physical significance, it points to new catalyst design. In the present case, the penultimate effect predicts that ES materials produced using **1** tend to cluster co-styrene in ES alternating sequences. This tendency results in styrene-rich regions and ethylene-rich regions along the polymer backbone. In other words these pseudo-random polymers have some pseudo-block character. The penultimate styrene effect in ES copolymerization also has been observed with zirconocene-based catalyst. For example, for ethylene-bis-indenyl-$ZrCl_2$ the values for r_{112} and r_{212} were found to be 111 and 14, respectively at 20 °C.[7b] It is not clear, however, if this enhanced styrene reactivity is due to modification of the active site by the aryl π-interaction of penultimate styrene or by favorable interaction between the penultimate styrene with incoming styrene monomer.

While **1** displays relatively high styrene reactivity ($r_{12}^{70°}$ = 23.0) with good overall catalyst efficiency, the styrene reactivity is insufficient for commercial operations. For comparison, the $r_{12}^{70°}$ values for propylene and octene copolymers with ethylene using catalyst **1** are 2.1 and 3.3, respectively,[15] indicating that styrene is an order of magnitude less reactive in co-ethylene polymerizations than propylene and octene. We desired new catalysts for the production of ES which show greatly improved styrene reactivity with comparable or improved catalyst efficiency. While not fully explaining the cause of the penultimate kinetic effect, it suggested to us that styrene reactivity may be improved if aryl substituents are positioned in the vicinity of the active site. To test this hypothesis, complexes **2** and **3** have been prepared, with aryl substituents placed in the 3 and 3′ positions of the Cp moiety and near the active site, and investigated for ES copolymerization performance.

Preparation of 2. The synthesis of 1,2-diphenylcyclopentadiene has been previously reported[16] as well as the synthesis of

(14) This assumption is not necessary for the kinetic modeling as described herein since the polymers possess reasonably high molecular weights, and end group effects are near zero. This is opposed to low molecular weight oligomers, where chemical shift differences may be observed due to differences in proximity to the end group.

(15) Unpublished results.

(16) (a) Guy, R.; Mahmoud, C. *Bull. Soc. Chim. Fr.* **1970**, *10*, 3585−3593. (b) Zhang, F.; Mu, Y.; Zhao Zhang, L., Y.; Bu, W.; Chen, C.; Zhai, H.; Hong, H. *J. Organomet. Chem.* **2000**, *613*, 68−76.

Scheme 5. Synthesis of Complex **2**

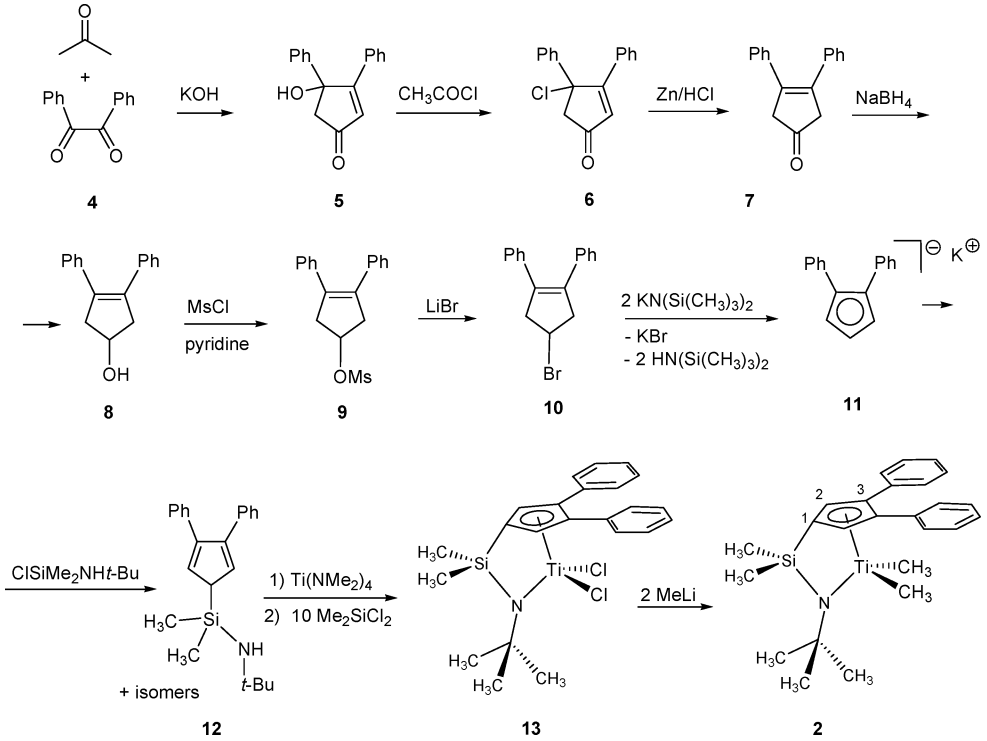

a zirconocene complex containing this ligand.[16b] The synthesis of 1,2-diphenyl-cyclopentadiene as reported herein differs from the published procedures and is outlined in Scheme 5. The first four steps of this synthesis (up to compound **8**) were performed by modification of procedures described in the literature,[17,18] whereas the synthesis of compound **10** follows that as described for 2-bromo-2,3-dihydro-1*H*-cyclopenta[*l*]phenanthrene.[19] Bromide **10** can be conveniently converted into monopotassium salt **11** by reaction with 2 equiv of $KN(Si(CH_3)_3)_2$ in toluene solution. In this particular case, the byproduct, KBr, was not separated from **11** as its presence does not interfere in the next synthetic step. Reaction of crude **11** with $ClSiMe_2$-NH-*t*-Bu in THF solution furnished ligand **12** as an orange oil. The ^{1}H NMR spectrum of compound **12** shows broad resonances which sharpen when heated to 60 °C. This suggests that **12** undergoes a fluxional process, presumably via a silatropic 1,5-shift.[20] Refluxing **12** with $Ti(NMe_2)_4$ in octane solution overnight gave a brown-red solution. Removal of solvent gave a red oil which was characterized by ^{1}H NMR spectroscopy to be the titanium bis(amide) complex in about 80% yield. In addition to the desired product, there was about 20% of a second possible isomer where the silicon bridge is attached to the 1-position of the Cp ring. The titanium bis(amide) complex was converted to the titanium dichloride, **13**, using Me_2SiCl_2 as the chlorinating agent in toluene solution. Removal of toluene followed by trituration of the final product with hexanes gave the desired complex **13** as the sole product. The other isomer presumably has higher hexane solubility and was washed away during the trituration. Treatment of **13** with 2 equiv of MeLi in hexane gave the desired complex **2** in 75% yield as a yellow crystalline solid. The ^{1}H NMR spectra of complexes **13** and **2** show a single resonance for the two silicon methyl groups and a single peak for the cyclopentadienyl protons which is consistent with the expected C_s symmetry of the two complexes. The two phenyl rings in **13** and **2** rotate rapidly on the NMR time scale in solution at room temperature as evidenced by the appearance of only four singlets for these phenyl rings in the $^{13}C\{^1H\}$ NMR spectrum.

Preparation of 3a/b. The synthesis of ligand **21** starting from phenanthrenequinone **14** is shown in Scheme 6. The first four steps of this synthesis (up to compound **17**) were performed by modification of procedures described in the literature.[19,21]

The potassium salt of the cyclopentaphenanthrenyl (CPPA) monoanion **18** was formed by reacting bromide **17** with 2 equiv of $KN(Si(CH_3)_3)_2$ in toluene solution. The precipitated product was separated from KBr by extraction with THF. The ^{1}H and $^{13}C\{^1H\}$ NMR spectra of **18** are consistent with the expected C_{2v} symmetry of this salt. The crystal structure of **18** was determined by single-crystal X-ray analysis. Reaction of **18** with an excess of dimethyldichlorosilane in THF solution gave a single monochloro derivative **19** in close to quantitative yield. There are two possible positional isomers, and each of those isomers potentially could have two double bond isomers as depicted in Scheme 7 (X = Cl).[22] Both ^{1}H and ^{13}C NMR spectra show two distinctly different resonances for the silyl methyl groups. This situation can only arise either if there is hindered rotation around the C^1-Si bond or if the entire molecule is chiral thus rendering both silyl methyl groups diastereotopic. Molecular modeling of **19** with a chlorodimethylsilyl group attached to

(17) Corey, E. J.; Uda, Hisashi. *J. Am. Chem. Soc.* **1963**, *85*, 1788−1792.
(18) See Supporting Information for details.
(19) Cooper, R. M.; Grossel, M. C.; Perkins, M. J. *J. Chem. Soc., Perkin Trans. 2* **1972**, 594−598.
(20) For silatropic shift in cyclopentadienyl derivatives, see: Rigby, S. S.; Gupta, H. K.; Werstiuk, N. H.; Bain, A. D.; McGlinchey, M. J. *Inorg. Chem. Acta* **1996**, *251*, 355−364.
(21) (a) Cope, A. C.; Field, L.; MacDowell, D. W. H.; Wright, M. E. *J. Am. Chem. Soc.* **1956**, *78*, 2547−2551. (b) Cope, A. C.; MacDowell, D. W. H. *J. Am. Chem. Soc.* **1958**, *80*, 5513−5516.
(22) In theory, silylation could also occur at a quaternary carbon in the Cp. However, due to steric effects this scenario is not very likely.

Scheme 6. Synthesis of Complexes **3a** and **3b**

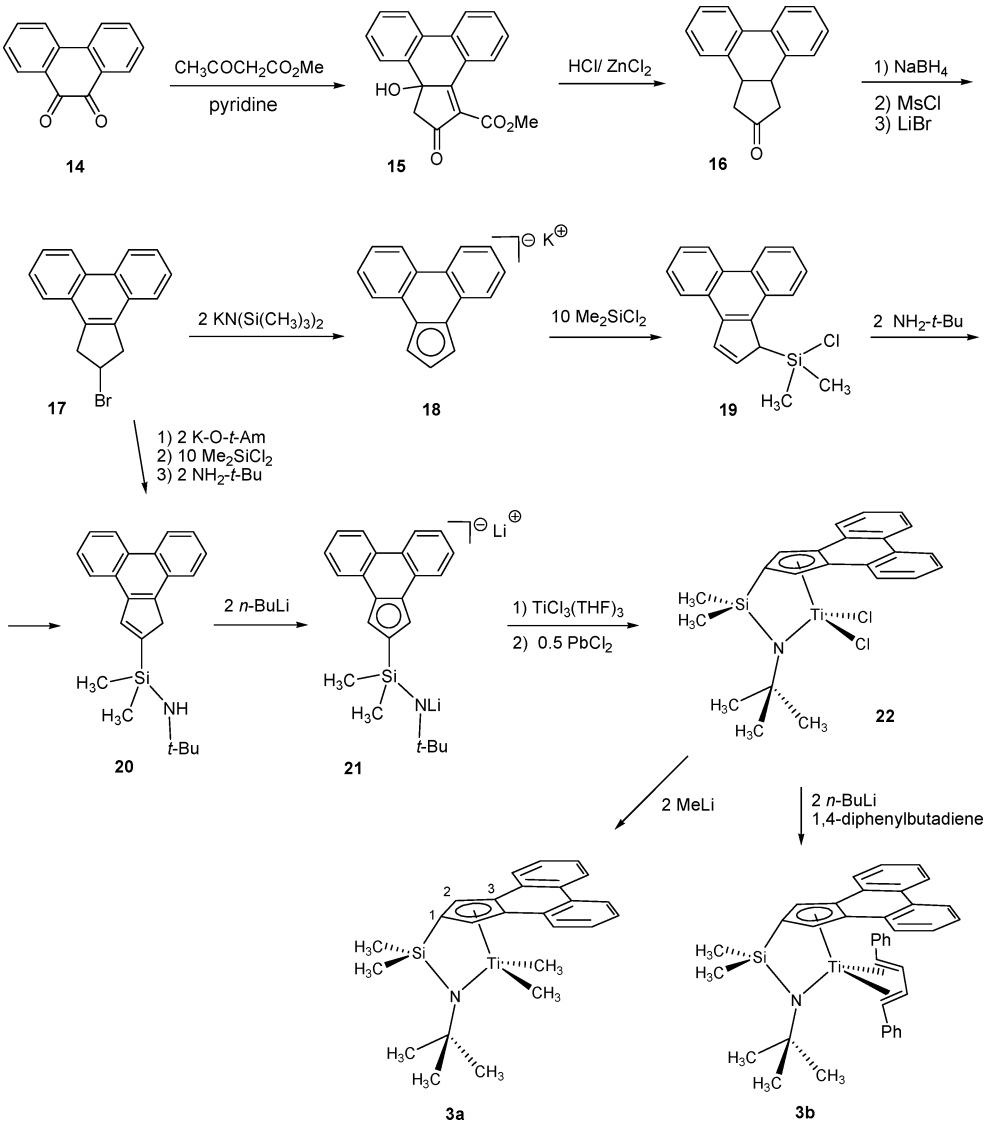

Scheme 7. Possible Isomers of CPPA-SiMe$_2$X Derivatives

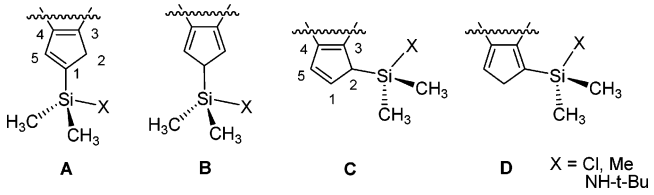

either the first or second position of the Cp fragment of CPPA does not suggest that there should be a high barrier for $C^{Cp}-Si$ bond rotation. This result points to molecular chirality as the reason for nonequivalency of the silyl methyl groups. Out of all four possible isomers only isomer **C** is chiral, and thus it is believed to be the product of the silylation reaction of **18**. Consistent with this analysis is the fact that the previously isolated trimethylsilyl derivative of CPPA was reported to have structure **C** (Scheme 7, X = Me).[23]

NOE experiments of **19** showed an EXSY cross-peak between protons at 4.16 (H2) and 7.35 (H5) ppm which indicates that they undergo chemical exchange presumably by [1,5]-silatropic shift as depicted in Scheme 8. Detailed kinetic analysis of this fluxional process was performed by magnetization

Scheme 8. Chemical Exchange via [1,5]-Silatropic Shift in **19**

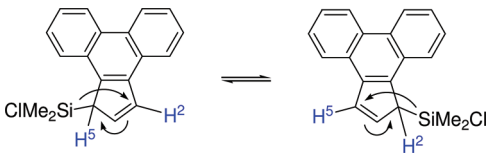

transfer using the DPFGSE-NOE method giving $\Delta H^{\ddagger} = 14.9(2)$ kcal/mol, $\Delta S^{\ddagger} = -11.4(6)$ eu.[18] These values are very similar to those obtained for the trimethylsilyl derivative of CPPA (X = Me).[23]

Ligand **20** can be synthesized either from **19** or directly from bromide **17**. Reaction of **19** with 2 equiv of *tert*-butylamine in toluene solution gives, after ammonium salt removal, ligand **20** in close to quantitative yield as a mixture of two isomers (9:1 ratio). A more convenient route to **20** involves reaction of bromide **17** with 2 equiv of potassium *tert*-amylate in THF (*in situ* formation of **18**) followed by reaction with 10 equiv of dichlorodimethylsilane (*in situ* formation of **19**) and finally reaction with *tert*-butylamine to yield product **20** in quantitative

(23) Rigby, S. S.; Gupta, H. K.; Werstiuk, N. H.; Bain, A. D.; McGlinchey, M. J. *Inorg. Chim. Acta* **1996**, *251*, 355−364.

Table 1. Selected Bond Lengths and Angles for **1**, **2**, **3a**, and **3b**

	1	2	3a	3b
Ti−C1	2.280(2)	2.298(2)	2.282(2)	2.221(3)
Ti−C2	2.348(2)	2.324(2)	2.358(2)	2.311(3)
Ti−C3	2.454(2)	2.475(2)	2.531(2)	2.515(3)
Ti−C4	2.454(2)	2.538(2)	2.513(2)	2.507(3)
Ti−C5	2.348(2)	2.399(2)	2.343(2)	2.310(3)
Ti−CH_3	2.125(2)	2.105(2)	2.111(3)	-
Ti−CH_3	2.125(2)	2.098(2)	2.109(3)	-
Ti−C24	-	-	-	2.190(3)
Ti−C25	-	-	-	2.312(3)
Ti−C26	-	-	-	2.300(3)
Ti−C27	-	-	-	2.207(3)
Ti−N	1.941(2)	1.934(2)	1.927(2)	1.976(2)
Si−N	1.746(1)	1.746(2)	1.750(2)	1.755(2)
Si−C1	1.874(3)	1.862(2)	1.864(3)	1.855(3)
C3−C12	-	1.476(2)	1.458(4)	1.442(4)
C4−C18	-	1.484(2)	1.453(3)	1.452(4)
C1−Si−N	94.4(3)	93.73(7)	93.0(1)	94.0(1)
Si−N−Ti	103.36(9)	102.80(8)	103.0(1)	99.5(1)
CH_3−Ti−CH_3	100.7(1)	100.5(1)	102.9(1)	-
C3−C4−C12	-	129.2(2)	120.6(2)	121.6(3)
C3−C4−C18	-	128.7(2)	121.0(2)	120.4(3)

Table 2. Important Structural Parameters for **1**, **2**, **3a**, and **3b**

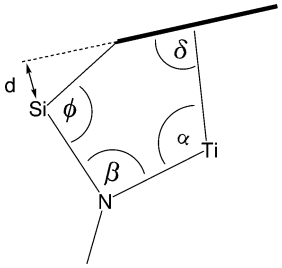

precatalyst	α	β	φ	δ	d	R(Ti−C_{cp}); Δr (Å)
1	108.5	103.4	92.4	84.3	0.91	2.280−2.454; 0.17
2	108.7	102.8	93.7	83.6	0.90	2.297−2.507; 0.21
3a	108.7	103.0	93.0	82.9	0.87	2.282−2.522; 0.24
3b	110.9	99.5	94.0	81.2	0.81	2.221−2.515; 0.29

yield. All three consecutive reactions are performed in the same reaction vessel with only solvent removal between steps. As in the case of **19**, there are four different possible isomers of ligand **20** (Scheme 7, X = NH-*t*-Bu). The ^{1}H and ^{13}C{^{1}H} NMR spectra of major isomer **20** show a single resonance for the silicon methyl groups indicating a lack of molecular chirality. Additionally, both ^{1}H NMR integration and inspection of the APT spectrum indicate the presence of a methylene group in the Cp portion of CPPA. The only two structures that match these requirements are **A** and **D** (Scheme 7, X = NH-*t*-Bu). NOESY1D experiments[18] are consistent only with structure **A**. The ^{1}H and ^{13}C{^{1}H} NMR spectra of the minor isomer are similar to those of **19** and show two nonequivalent silyl methyl peaks indicating structure **C** for this isomer. Reaction of **20** with 2 equiv of *n*-butyl lithium in benzene solution gave desired dilithium salt **21** in quantitative yield. Syntheses of the metal complexes **22** and **3a,b** are shown in Scheme 6. The titanium dichloride derivative **22** was synthesized in a standard procedure by reacting **21** with $TiCl_3$ in THF solution followed by oxidation with lead chloride. A single resonance for the silyl methyl groups in both the ^{1}H and ^{13}C{^{1}H} NMR spectra of **22** is consistent with C_s symmetry for the complex. The total number of aromatic carbon resonances is half +1 (9 in all) of that observed in the C_1 symmetric ligand **20**. Reaction of **22** with 2 equiv of MeLi

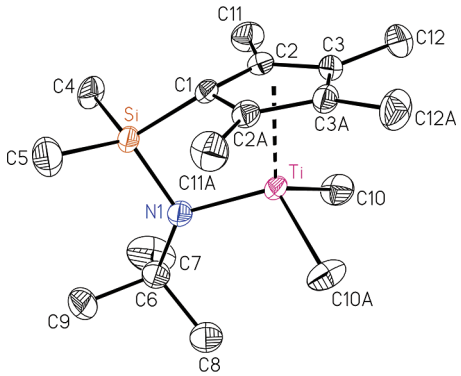

Figure 6. Thermal ellipsoid drawing of **1** shown at the 40% probability level. Hydrogen atoms have been omitted for clarity.

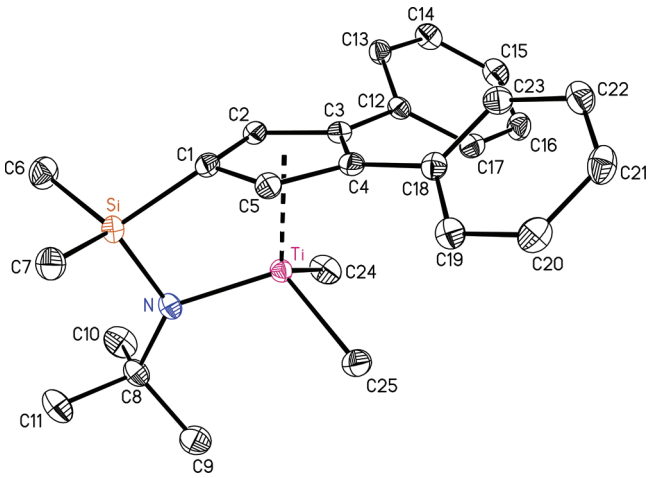

Figure 7. Thermal ellipsoid drawing of **2** shown at the 40% probability level. Hydrogen atoms have been omitted for clarity.

in toluene solution provided **3a** in good yield. Treatment of **22** with 2 equiv of *n*-BuLi in the presence of *trans*,*trans*-1,3-diphenylbutadiene gave complex **3b** in high yield.[24]

X-ray Crystal Structure of Complexes 1, 2, 3a, and 3b. Surprisingly, examination of the solid-state structures of the catalyst complexes discussed herein does not show appreciable changes in the titanium coordination geometry to account for the large differences in polymerization performance. Crystals of **1**[25] and **2** suitable for X-ray analysis were obtained from saturated hexane solutions at −30 °C. Complexes **1** and **2** crystallize in orthorhombic (*Pnma*) and monoclinic ($P2_1/c$) space groups, respectively. In the case of **3a** and **3b**, crystals suitable for X-ray analysis were grown from toluene/hexane mixtures (**3a**) at −27 °C and by slow benzene evaporation (**3b**) at room temperature. Both complexes crystallize in a triclinic ($P\bar{1}$) space group with two independent molecules in the asymmetric unit. Selected bond lengths and angles for **1**, **2**, **3a**, and **3b** are shown in Table 1, and important structural parameters are depicted in Table 2. The thermal ellipsoid drawings of **1**, **2**, **3a**, and **3b** are presented in Figures 6, 7, 8, and 9, respectively. The titanium atom is in a pseudo-tetrahedral environment defined by the η^5-bound Cp fragment, the σ-bound amido ligand, and the two methyl or diene (for **3b**) groups. Diphenylbutadiene adopts a prone-s-*cis* configuration in **3b** with the four butadiene carbon

(24) Devore, D. D.; Timmers, F. J.; Hasha, D. L.; Rosen, R. K.; Marks, T. J.; Deck, P. A.; Stern, C. L. *Organometallics* **1995**, *14*, 3132−3134.
(25) A lower quality structure of **1** has recently been published. Nishii, K.; Ikeda, T.; Akita, M.; Shiono T. *J. Mol. Catal. A: Chem.* **2005**, *231*, 241−246.

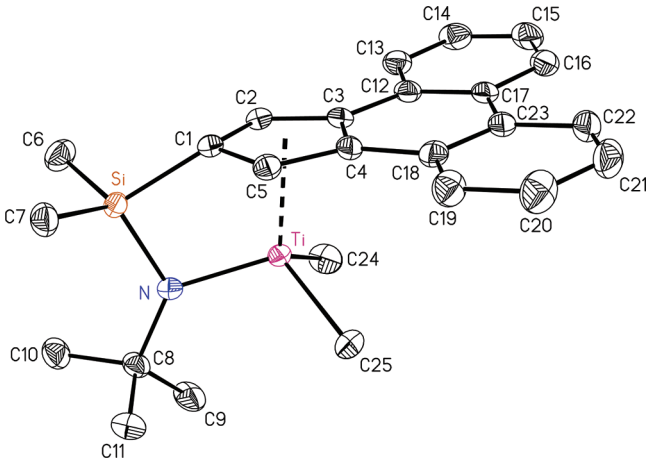

Figure 8. Thermal ellipsoid drawing of **3a** shown at the 40% probability level. Hydrogen atoms have been omitted for clarity.

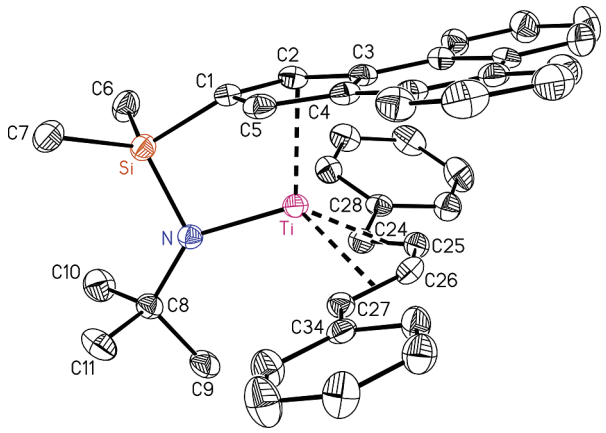

Figure 9. Thermal ellipsoid drawing of **3b** shown at the 40% probability level. Hydrogen atoms have been omitted for clarity.

atoms (C24−C27) adopting a coplanar arrangement (with the largest deviation from the least-square plane of only 0.016 Å for C25). One phenyl ring defined by atoms C34−C39 is almost coplanar with the butadiene unit with a dihedral angle between planes of 2.7°. The plane of the second phenyl ring (C28−C33), however, is rotated by 32.3° from the plane defined by the butadiene carbon atoms. The Δd (the distance difference between the average Ti−C(terminal diene carbons) and the average Ti−C(internal diene carbons)) for the diene ligand is −0.108 Å which supports the assignment of a predominantly π-bound diene ligand.[24,26] Unlike the phenanthrene fragment in complexes **3a** and **3b**, which are planar and coplanar with the Cp portion of the ligand, the two phenyl groups in **2** are rotated in the same direction relative to the Cp ring. The dihedral angles between the plane of Cp and the planes of the phenyl rings are 34.0° and 35.3°. Key bond distances (Table 1) and skeletal angles such as centroid−Ti−N1, Ti−N1−Si, and N1−Si−C1 (Table 2) are found to be very similar in **1**, **2**, and **3a** suggesting that the carbon-based cyclopentadienyl substitution[27] does not play a major role in effecting the coordination environment around the titanium atom in these complexes. In fact, the largest structural differences are observed between **3a** and **3b**, complexes having the same CGC ligand. This indicates that the geometry change from **3a** to **3b** is caused by the presence of the large diphenylbutadiene ligand. While the geometries around the Ti centers are very similar in complexes **1**, **2**, and **3a**, the steric differences between 3 and 3′ cyclopentadienyl substituents are very distinct. The constraining effect of these types of CGC ligands dictates the geometry around Ti, while the Cp substituents can influence both steric and electronic properties of the catalyst.

Batch Polymerization Screening. Complexes **1**, **2**, **3a**, and **3b** were evaluated in ethylene−styrene copolymerization at 90 °C and 200 psi ethylene pressure using a 2 L semibatch reactor (Table 3). The results shown in Table 3 indicate that both complexes **2** and **3** show a significant improvement compared to catalyst **1** with regard to efficiency, styrene reactivity, and polymer molecular weight.[28] It is clear that the placement of aryl groups in close proximity to the active site has a beneficial influence on the performance of these new catalysts thereby confirming the initial hypothesis. Complex **2** is, however, less efficient (65%) and less reactive toward styrene (22 vs 31 mol % co-styrene) than **3** under the conditions studied. Presumably, the freely rotating phenyl groups in **2** offer an increased steric profile to the incoming bulky styrene monomer leading to lower styrene reactivity compared to catalysts **3a**/**3b**.[29] However, the importance of an electronic influence should not be discounted. The permanently coplanar aryl groups of **3** can be more effective electron donors to the Cp moiety through conjugation than can the phenyl groups of **2** which can rotate out of coplanarity.[27a] While several cyclopentadienyl- and indenyl-based CGC complexes were investigated[4] in ES copolymerization, none exhibited the high styrene reactivity and polymerization activity of **3**.

Table 3. Ethylene−Styrene Copolymerization Results for **1**, **2**, and **3a**[a]

procatalyst	polymer yield (g)	efficiency, g(polymer)/g(Ti)	mole % S	wt % aPS	Mw	Mw/Mn
1	35.6	248 000	11.0%	0.73%	11 300	2.36
2	91.5	637 000	21.5%	1.48%	72 800	4.76
3a	149.1	1 038 000	30.6%	0.87%	134 100	5.26

[a] Activator $B(C_6F_5)_3$, precatalyst amount = 3 μmol, activator amount = 9 μmol, 455 g of styrene, 433 g of toluene, ethylene = 200 psi, run time 30 min, temp = 90 °C, Δ psi H_2 = 50.

Steady-State Kinetic Modeling of 3b for ESI. A first-order Markovian (simple) kinetic model was sufficient to accurately fit the six ^{13}C NMR peak regions for the ES materials produced.[30] No erosion of the fit accuracy was observed as a function of composition such that a penultimate model was not

(26) For other Ti−diphenylbutadiene complexes, see: (a) Spencer, M. D.; Wilson, S. R.; Girolami, G. S. *Organometallics* **1997**, *16*, 3055−3067. (b) Abboud, K. A.; Nickias, P. N.; Chen, E. Y.-X. *Acta Crystallogr., Sect. C* **2001**, *C57*, 1408−1409.

(27) Heteroatom Cp and indenyl substitution was shown to exert a considerable electronic effect on the geometry of CGC complexes: (a) Klosin, J.; Kruper, W. J., Jr.; Nickias, P. N.; Roof, G. R.; De Waele, P.; Abboud, K. A. *Organometallics* **2001**, *20*, 2663−2665. (b) Grandini, C.; Camurati, I.; Guidotti, S.; Mascellani, N.; Resconi, L.; Nifant'ev, I. E.; Kashulin, I. A.; Ivchenko, P. V.; Mercandelli, P.; Sironi, A. *Organometallics* **2004**, *23*, 344−360. (c) Ryabov, A. N.; Voskoboynikov, A. Z. *J. Organometal. Chem.* **2005**, *690*, 4213−4221.

(28) Both **2** and **3** were found to be somewhat less efficient than **1** in ethylene/1-octene polymerization processes. Octene reactivity was found to be comparable for **1** and **2** but much higher for **3** which is consistent with **3** offering a less congested active site. Interestingly, while the molecular weight of ES polymers was found to be the highest for **3** and the lowest for **1**, the molecular weight trend is reversed for EO polymerization. See Supporting Information for details.

(29) Catalysts **3a** and **3b** exhibit comparable ES polymerization performance.

(30) See Supporting Information for details.

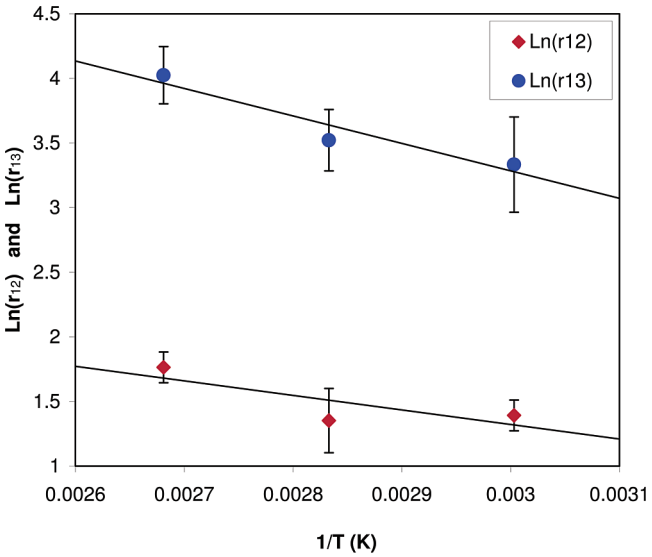

Figure 10. ES first-order Arrhenius plot for **3b** using the simple kinetic model.

Scheme 9. Kinetic Parameters for **3b** (70 °C) Using First-Order Markovian (Simple) Kinetic Model

$$r_{12}^{70^\circ} = 4.16 \qquad r_{12} = 4.16 \exp\left[\frac{-2069}{1.987}\left(\frac{1}{T} - \frac{1}{343\ K}\right)\right]$$

$$r_{13}^{70^\circ} = 34.8 \qquad r_{13} = 34.8 \exp\left[\frac{-2069}{1.987}\left(\frac{1}{T} - \frac{1}{343\ K}\right)\right]$$

$$R^{70^\circ} = 0.0004 \qquad E_{12} = 2069\ \text{cal/mol}$$

necessary. Presumably, the influence of the CPPA aryls overwhelms any aryl group influence on the growing polymer chain. The optimal 70 °C kinetic parameters for **3b** (extrapolated) are shown in Scheme 9, and the Arrhenius plot for this model is shown in Figure 10. The r_{12} value 4.4 for **3b** is in agreement with the improved styrene reactivity observed in the batch polymerization screen (Table 3) and compares very favorably with an r_{12} for **1** of 23.1. It is also interesting to note that the r_{12} for **3b** is much less dependent on temperature than that for **1** indicating that an ESI polymerization process using **3b** can be run at higher temperatures without sacrificing styrene reactivity.

In this kinetic model for catalyst **3b**, it is curious that the fit is much more dependent on r_{13} than reactivity ratio R which is contrary to what was observed for catalyst **1**. This kinetic result for **3b** suggests that the sequence that gives rise to the $\alpha\beta$ methylene signal is predominantly from the $S_{21}-E-S_{12}$ sequence rather than from the $S_{12}-S_{21}$ sequence.

As noted above, a penultimate effect was not observed in ES materials prepared using **3**. While the microstructure is still best described as pseudo-random, differences in the microstructure must exist in ES prepared using **1** versus **3** based upon the optimal kinetic models for these two catalysts. A rapid and quantitative method based upon empirical data only was desired to describe the differences in microstructure for these and other ES materials and to serve as yet another means to evaluate catalyst performance. The penultimate phenomenon for polymerization processes involving catalyst **1** results in increased clustering of co-styrene units into alternating ethylene−styrene sequences in ES materials resulting in fewer isolated co-styrene units at the same co-styrene composition compared to **3**. Increased styrene clustering in alternating sequences will result in an increase in the number of $\beta\beta$ methylene carbons (SES sequences) at the expense of more isolated β methylene carbons. These methylene carbons are clearly resolved in the $^{13}C\{^1H\}$ NMR spectrum of ES materials, ca. 26 and 28 ppm for SES and isolated styrene triads, respectively (Figure 2). A ratio of these peak areas, NMR_{26}^{SES}/NMR_{28}, will give an indication of the tendency of styrene units to be clustered; the higher this ratio, the greater the tendency to cluster in alternating runs. However, this ratio is also composition dependent. As the co-styrene composition increases, one would naturally expect the ratio to increase as the styrene units get closer together along the chain. A clustering index, CI_{pr}, for pseudo-random copolymers was derived which is based on the empirical NMR ratio but also attempts to account for the composition dependence of this peak area ratio. The cluster index is based on simple hypothetical ES kinetics with only one reactivity ratio, r_{12}, and no inverse styrene insertion. For this hypothetical pseudo-random case, the NMR peak area ratio is derived to be a function only of copolymer composition, eq 1,

$$\frac{{}^*NMR_{26}^{SES}}{{}^*NMR_{28}} = \frac{1 - F_1}{4F_1 - 2} \tag{1}$$

where the asterisk (*) denotes hypothetical kinetics and F_1 is the copolymer mole fraction of ethylene.

The pseudo-random cluster index, CI_{pr}, is defined as the observed NMR peak ratio divided by this hypothetical ratio, eq 2.

$$CI_{pr} = \left(\frac{NMR_{26}^{SES}}{NMR_{28}}\right)\left(\frac{4F_1 - 2}{1 - F_1}\right) \tag{2}$$

Thus, the empirically derived cluster index is dependent only on the integrated area of two NMR peaks and the composition of the copolymer which is also determined via the NMR spectrum. The hypothetical copolymer is perfectly random within the pseudo-random constraint, and its CI_{pr} value is 1.0. A CI_{pr} less than 1 indicates the comonomer distribution is more evenly distributed than the hypothetical polymer, whereas a value greater than 1 indicates the styrene units are more clustered in ES alternating runs than the hypothetical polymer.

A plot of the CI_{pr} versus copolymer composition for ESI materials prepared using different catalysts is shown in Figure 11. For ESI prepared using catalyst **3b** it is clear that the CI_{pr} remains less than 1 over the composition range studied. The CI_{pr} of the ESI prepared using **1** are greater than 1, as expected, but it also remains a steep function of copolymer composition and approaches 1 only as the composition approaches 50 mol % styrene (79 wt %).

The difference in copolymer microstructure for ES materials prepared using **1** versus **3** might manifest itself in physical properties of the copolymers. One may expect that the clustering of styrene in alternating ES sequences with concomitant longer ethylene runs will result in higher copolymer melting points and Tg's at comparable compositions for ES prepared with **1** vs **3**. Measured property differences were found to be small, however.

Conclusions

Kinetic measurements of ethylene−styrene copolymerization experiments catalyzed by CGC catalyst **1** revealed that the

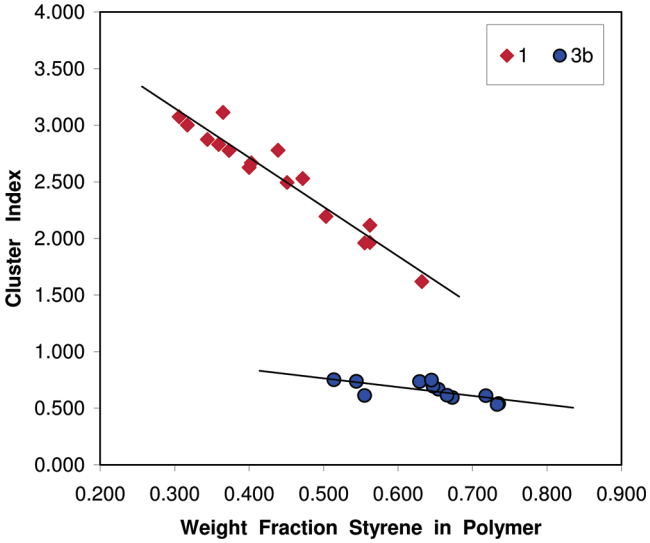

Figure 11. CI_{pr} versus copolymer composition for various ESI materials

inherent reactivity of **1** toward styrene is improved when the penultimate monomer on the growing polymer chain is styrene rather than ethylene. The penultimate styrene effect clearly indicates that the presence of next-to-last styrene lowers the styrene insertion barrier relative to that of ethylene. It is not clear, however, if this effect is due to next-to-last styrene interaction with the cationic metal center, interaction with incoming styrene, or both of these effects. Nevertheless, the presence of this effect suggests that properly modified catalyst ligand structures with aryl groups positioned in close proximity to the active center might lead to their positive interaction with incoming styrene thus further lowering the styrene insertion barrier (enhancement of styrene reactivity). To explore this possibility, two new CGC catalysts were prepared, one having two phenyl substituents placed in the 3 and 3′ positions of the Cp ring (**2**) and the other with a 2,2′-biphenyl fragment attached to the Cp ring (**3**), also at the 3 and 3′ positions. Kinetic measurements revealed clustering into alternating ES sequences for catalyst **1**, whereas **3** showed more even monomer distributions. Ethylene styrene copolymerization studies demonstrated that both catalysts **2** and **3** lead to polymers with substantially enhanced styrene content relative to **1** under the same polymerization conditions. Catalyst **3** in particular showed remarkable styrene reactivity, with nearly a 6-fold increase in the styrene reactivity in ES copolymerization processes at 70 °C compared to **1**. Additionally, **3** was found to be four times as active as **1** when compared under the same polymerization conditions. Outstanding polymerization characteristics achieved with **3** make this catalyst the current state-of-the-art for ES copolymerization and a viable candidate for commercial production of ethylene–styrene resins in a solution process.

Experimental Section

General Considerations. All syntheses and manipulations of air-sensitive materials were carried out in an inert atmosphere (nitrogen or argon) glove box. Solvents were first saturated with nitrogen and then dried by passage through activated alumina and Q-5 (available from Engelhardt Chemicals Inc.) catalyst prior to use.[31] Benzene-d_6 was dried over sodium/potassium alloy and filtered prior to use. THF-d_8, $CDCl_3$, and $C_2D_2Cl_4$ (from Cambridge Isotopes) were used as received. NMR spectra were recorded on either a Varian INOVA 300 or Mercury Vx 300 (FT 300 MHz, ^{1}H; 75 MHz, ^{13}C) spectrometer. ^{1}H NMR data are reported as follows: chemical shift (multiplicity (br = broad, s = singlet, d = doublet, t = triplet, q = quartet, p = pentet, and m = multiplet), integration, and assignment). Chemical shifts for ^{1}H NMR data are reported in ppm downfield from internal tetramethylsilane (TMS, δ scale) using residual protons in the deuterated solvents (C_6D_6, 7.15 ppm: $CDCl_3$, 7.25 ppm, $C_2D_2Cl_4$, 5.99 ppm, THF-d_8, 1.73, 3.58 ppm) as references. ^{13}C NMR data were determined with ^{1}H decoupling, and the chemical shifts are reported in ppm vs tetramethylsilane (C_6D_6, 128 ppm, $CDCl_3$, 77 ppm, $C_2D_2Cl_4$, 73.8 ppm, THF-d_8, 25.3, 67.4 ppm). Coupling constants are reported in hertz (Hz). Mass spectra (both positive and negative FAB) were recorded on a VG Autospec (S/N V190) mass spectrometer. Elemental analyses were performed by University of Michigan analytical services and Oneida Research Services, Inc., Whitesboro, NY.

Preparation of Dichloro[*N*-(1,1-dimethylethyl)-1,1-dimethyl-1-[(1,2,3,4,5-η)-3,4-diphenyl-2,4-cyclopentadien-1-yl]silanaminato-(2-)-κN]-titanium (13). The *N*-(*tert*-butyl)(3,4-diphenyl-2,4-cyclopentadien-1-yl)dimethylsilanamine (**12**) (2.33 g, 6.71 mmol) and $Ti(NMe_2)_4$ (1.50 g, 6.71 mmol) were dissolved in octane (50 mL). The solution was refluxed overnight. The color changed from orange to deep red. The solvent was removed under reduced pressure to give a thick red oil (3.23 g). The ^{1}H NMR spectrum showed formation of the desired bis(amido) complex [^{1}H (C_6D_6) δ 0.60 (s, 6H, $Si(CH_3)_2$), 1.39 (s, 9H, $C(CH_3)_3$), 2.83 (s, 12H, $Ti(N(CH_3)_2)_2$), 6.33 (s, 2H, H2), 7.07 (m, 6H), 7.45 (m, 4H)] in about 75% yield. To the red oil dissolved in toluene (40 mL) was added Me_2SiCl_2 (8.6 g). After the mixture stirred for 2 days, the solvent was removed under reduced pressure leaving a dark solid. Hexane (50 mL) was added, and the mixture was stirred for 3 h. A green-yellow solid was collected on a frit, washed with cold hexane (20 mL), and dried under reduced pressure to give 1.66 g of product. The yield was 75.0%. NMR spectroscopy showed the presence of only the desired complex. Recrystallization: The final product (0.71 g) was dissolved in toluene (10 mL) followed by hexane (50 mL). After 2 min the solution was filtered and put aside at room temp. After a few minutes yellow crystals appeared. After 5 h at room temperature the solution was put into a freezer overnight (−27 °C). The solvent was decanted, and the crystals were washed with cold hexane (15 mL) to give 0.512 g of product. ^{1}H (C_6D_6) δ 0.32 (s, 6H, $Si(CH_3)_2$), 1.42 (s, 9H, $C(CH_3)_3$), 6.51 (s, 2H, H2), 7.02 (m, 6H), 7.54 (m, 4H). $^{13}C\{^1H\}$ (C_6D_6) δ −0.10 ($Si(CH_3)_2$), 32.57 ($C(CH_3)_3$), 64.46 ($C(CH_3)_3$), 110.00 (C1), 126.27, 128.38, 128.72, 130.13, 133.98, 141.37. HRMS (EI, $(M-CH_3)^+$): calcd for $C_{22}H_{22}NSiTiCl_2$ 448.0534, found 448.0534. Anal. Calcd for $C_{23}H_{25}NSiTiCl_2$: C, 59.49; H, 5.86; N, 3.02. Found: C, 59.25; H, 5.95; N, 3.42. The ^{1}H and $^{13}C\{^1H\}$ NMR spectra of this material are shown in the Supporting Information.

Preparation of [*N*-(1,1-Dimethylethyl)-1,1-dimethyl-1-[(1,2,3,4,5-η)-3,4-diphenyl-2,4-cyclopentadien-1-yl]silanaminato(2-)-κN]-dimethyl-titanium (2). In the drybox dichloro-[*N*-(1,1-dimethylethyl)-1,1-dimethyl-1-[(1,2,3,4,5-η)-3,4-diphenyl-2,4-cyclopentadien-1-yl]silanaminato(2-)-κN]-titanium complex (**13**) (0.41 g, 0.89 mmol) was dissolved in toluene (30 mL). To this solution MeLi (1.2 mL, 1.6 M in ether, 1.91 mmol) was added dropwise with stirring over a 1 min period. After the addition of MeLi was completed, the solution was stirred for 45 min. Volatile components were removed under reduced pressure, and the residue was extracted with hot hexane (35 mL). The solution was filtered hot and put into a freezer overnight. The solvent was decanted, and the yellow crystals were washed with cold hexane and then dried under reduced pressure to give 0.272 g of product. Yield 74.5% ^{1}H (C_6D_6) δ 0.34 (s, 6H, $Si(CH_3)_2$), 0.78 (s, 6H, $Ti(CH_3)_2$), 1.56 (s, 9H, $C(CH_3)_3$), 6.18 (s, 2H, H2), 7.04 (m, 2H, para), 7.08 (m, 2H, meta), 7.49 (m, 4H, ortho). $^{13}C\{^1H\}$ (C_6D_6) δ 0.85 ($Si(CH_3)_2$), 34.54 ($C(CH_3)_3$), 56.27 (q, $^1J_{C-H}$ = 120.06 Hz, $Ti(CH_3)_3$), 59.68 ($C(CH_3)_3$), 104.88 (C1), 122.80 (*C*2), 127.56 (para), 128.49 (meta), 129.55 (ortho),

(31) Pangborn, A. B.; Giardello, M. A.; Grubbs, R. H.; Rosen, R. K.; Timmers, F. J. *Organometallics* **1996**, *15*, 1518−1520.

135.39, 135.90. Peak assignments were performed based on HSQC and NOESY spectra. HRMS (EI, $(M-CH_3)^+$): calcd for $C_{24}H_{30}NSiTi$ 408.1627, found 408.1624. Anal. Calcd for $C_{25}H_{33}NSiTi$: C, 70.90; H, 7.85; N, 3.31. Found: C, 70.64; H, 7.91; N, 3.06. The ^1H and $^{13}C\{^1H\}$ NMR spectra of this material are shown in the Supporting Information.

Preparation of Dichloro-[1-[(1,2,3,3a,11b-η)-1*H*-cyclopenta[*l*]-phenanthren-2-yl]-*N*-(1,1-dimethylethyl)-1,1-dimethylsilanaminato-(2-)-κN]-titanium (22). To a 250 mL round bottom flask containing $TiCl_3(THF)_3$ (1.17 g, 3.00 mmole) and THF (about 120 mL) was added at a fast drip rate a THF solution of [2-[[(1,1-dimethylethyl)amino]-dimethylsilyl]-1*H*-cyclopenta[*l*]phenanthren-1-yl]-lithium (**21**) (1.08 g in 50 mL). The mixture was stirred at about 20 °C for 1.5 h at which time solid $PbCl_2$ (0.55 g, 2.0 mmol) was added. After stirring for an additional 1.5 h, the THF was removed under vacuum and the residue was extracted with toluene, filtered, and dried under reduced pressure to give an orange solid. Yield was 1.31 g (93.5%). ^1H (CD_2Cl_4) δ 0.78 (s, 6H, Si(CH_3)$_2$), 1.42 (s, 9H, C(CH_3)$_3$), 7.09 (s, 2H, H2), 7.65 (m, 2H, H4), 7.69 (td, 2H, H5), 8.18 (dm, 2H, $^3J_{H-H}$ = 6.9 Hz, H3), 8.52 (dm, 2H, $^3J_{H-H}$ = 7.8 Hz, H6). $^{13}C\{^1H\}$ (CD_2Cl_4) δ 0.44, 32.80, 65.24, 112, 32 (C1), 118.63 (C2), 123.94, 126.37, 126.97 (quat.), 127.96, 129.22, 130.85 (quat.), 133.71 (quat.). Anal. Calcd for $C_{23}H_{25}Cl_2NSiTi$: C, 59.75; H, 5.45; N, 3.03. Found: C, 59.40; H, 5.67; N, 2.75. The ^1H and $^{13}C\{^1H\}$ NMR spectra of this material are shown in the Supporting Information.

Preparation of [1-[(1,2,3,3a,11b-η)-1*H*-Cyclopenta[*l*]phenanthren-2-yl]-*N*-(1,1-dimethylethyl)-1,1-dimethylsilanaminato(2-)-κN]-dimethyl-titanium (3a). In a drybox dichloro[1-[(1,2,3,3a,11b-η)-1*H*-cyclopenta[*l*]phenanthren-2-yl]-*N*-(1,1-dimethylethyl)-1,1-dimethylsilanaminato(2-)-κN]-titanium complex (**22**) (1.37 g, 2.96 mmol) was suspended in toluene (40 mL). To this mixture MeLi (1.6 M in ether, 3.9 mL, 6.2 mmol) was added dropwise over a 1 min period while stirring. After the addition of MeLi was completed, the solution was stirred for 2 h. Toluene was removed under reduced pressure, and the residue was extracted with a hot mixture of hexane (40 mL) and toluene (7 mL). The solution was filtered hot and put into a freezer overnight. Solvent was decanted, and the yellow crystalline material was washed with cold hexane (3 × 10 mL) and then dried under reduced pressure to give ca. 0.8 g of product. Solvent was removed under reduced pressure from the decanted solution, and the residue was dissolved in boiling hexane (20 mL) and then filtered. The solution was put into a freezer overnight. The solvent was decanted, and the yellow crystals were washed with cold hexane (5 mL) and then dried under reduced pressure to give 0.155 g of product. Yield 76.5%. ^1H (C_6D_6)) δ 0.22 (s, 6H, Si(CH_3)$_2$), 0.43 (s, 6H, Ti(CH_3)$_2$), 1.49 (s, 9H, C(CH_3)$_3$), 6.63 (s, 2H, H2), 7.32 (td, 2H, $^3J_{H-H}$ = 7.2 Hz, $^4J_{H-H}$ = 1.5 Hz, H5), 7.36 (td, 2H, $^3J_{H-H}$ = 7.2 Hz, $^4J_{H-H}$ = 1.5 Hz, H4), 7.90 (dm, 2H, $^3J_{H-H}$ = 6.9 Hz, H3), 8.27 (dm, 2H, $^3J_{H-H}$ = 7.2 Hz, H6). $^{13}C\{^1H\}$ (C_6D_6) δ 0.85 (Si(*C*H_3)$_2$), 34.57 (C(*C*H_3)$_3$), 56.73 (q, $^1J_{C-H}$ = 120.06 Hz, Ti-(*C*H_3)$_2$), 59.73 (*C*(CH$_3$)$_3$), 107.33 (C1), 113.72 (C2), 124.10 (C6), 125.31 (C3), 127.29 (C5), 127.55 (C4), 128.78, 129.42, 130.25. Peak assignments were performed based on HSQC and NOESY spectra. HRMS (EI, $(M-CH_3)^+$): calcd for $C_{24}H_{28}SiNTi$ 406.1470, found 406.1473. Anal. Calcd for $C_{25}H_{31}NSiTi$: C, 71.24; H, 7.41; N, 3.32. Found: C, 70.81; H, 7.48; N, 3.07. The ^1H and $^{13}C\{^1H\}$ NMR spectra of this material are shown in the Supporting Information.

Preparation of [1-[(1,2,3,3a,11b-η)-1*H*-cyclopenta[*l*]phenanthren-2-yl]-*N*-(1,1-dimethylethyl)-1,1-dimethylsilanaminato(2−)-κN](1,4-diphenyl-1,3-butadiene-1,4-diyl)-titanium (3b). To a warm (65 °C) slurry of dichloro[1-[(1,2,3,3a,11b-η)-1*H*-cyclopenta[*l*]phenanthren-2-yl]-*N*-(1,1-dimethylethyl)-1,1-dimethylsilanaminato(2-)-κN]-titanium (**22**) (8.65 g, 0.0187 mol) and *trans*,*trans*-1,4-diphenylbutadiene (3.94 g, 0.0191 mol) in toluene (about 200 mL) was added *n*-BuLi (25 mL of a 1.6 M solution, 0.040 mol). The solution darkened immediately, and the temperature climbed to 72 °C. After ca. 45 min, the temperature was increased to bring the mixture to reflux, and the mixture was maintained at that temperature for 1.5 h. The mixture was cooled to about room temperature, and the volatiles were removed under reduced pressure. The residue was slurried in mixed hexanes (60 mL) at about 20 °C for approximately 16 h. The mixture was cooled to about −25 °C for about 1 h. The solids were collected on a glass frit by vacuum filtration and dried under reduced pressure. The dried solid was placed in a glass fiber thimble, and the solid was extracted continuously with hexanes using a Soxhlet extractor. After 6 h a dark crystalline solid was observed in the boiling pot. The mixture was cooled to about −20 °C, and the solid was isolated by filtration from the cold hexanes and dried under reduced pressure to give 6.65 g of a dark crystalline solid. The filtrate was discarded. The solids in the extractor were stirred, and the extraction continued with an additional quantity of mixed hexanes. After 8 h of extraction, crystals had formed in the boiling hexanes once again. These were isolated to give an additional 2.05 g of the desired product as a dark crystalline solid. The combined yield was 8.70 g, 78%. ^1H (C_6D_6) δ 0.70 (s, 6H, Si(CH_3)$_2$), 1.21 (s, 9H, C(CH_3)$_3$), 3.23 (m, H25/H26), 3.76 (m, H24/H27), 6.71 (s, 2H, H2), 6.95−7.18 (m, 14H), 7.24 (ddd, 2H, $^3J_{H-H}$ = 8.3 Hz, $^3J_{H-H}$ = 6.6 Hz, $^4J_{H-H}$ = 1.5 Hz), 8.10 (d, 2H, $^3J_{H-H}$ = 8.1 Hz). $^{13}C\{^1H\}$ (C_6D_6) δ 2.47 (Si(*C*H_3)$_2$), 35.58 (C(*C*H_3)$_3$), 58.75 (*C*(CH$_3$)$_3$), 87.81 (dm, $^1J_{C-H}$ = 134.0 Hz, C24/C27), 106.40 (d, $^1J_{C-H}$ = 162.2 Hz, C25/C26), 110.82 (dd, $^1J_{C-H}$ = 172.2 Hz, $^2J_{C-H}$ = 8.5 Hz, *C*2/C5), 111.19 (quat.), 123.39, 124.49, 125.40, 125.98 (quat.), 126.67, 127.11, 127.24, 127.77 (quat.), 128.22, 129.24 (quat.), 142.75 (quat.). HRMS (EI, M^+): calcd for $C_{39}H_{39}SiNTi$ 597.2331, found 597.2324. Anal. Calcd for $C_{39}H_{39}SiNTi$: C, 78.37; H, 6.58; N, 2.34. Found: C, 77.55; H, 6.39; N, 1.82. The ^1H and $^{13}C\{^1H\}$ NMR spectra of this material are shown in the Supporting Information.

Structure 1. $C_{17}H_{33}NSiTi$, Mw = 327.43, orthorhombic, *Pnma*, yellow plate (0.36 × 0.32 × 0.10 mm^3), a = 11.8100(8) Å, b = 13.3721(9) Å, c = 12.2118(8) Å, temp = 173(2) K, Z = 4, V = 1928.5-(2) Å^3, R1 = 0.0336, 0.0398, wR2 = 0.0951, 0.0990 ($I > 2\sigma(I)$, all data), GOF = 1.068.

Structure of 2. $C_{25}H_{33}NSiTi$, Mw = 423.51, monoclinic, *P*2(1)/*c*, yellow plate (0.30 × 0.19 × 0.08 mm^3), a = 22.958(2) Å, b = 8.1979-(6) Å, c = 12.4332(9) Å, β= 97.321(1)°, Z = 4, V = 2321.0(3) Å^3, R1 = 0.0371, 0.0455, wR2 = 0.0949, 0.1011 ($I > 2\sigma(I)$, all data), GOF = 1.048.

Structure of 3a. $C_{25}H_{31}NSiTi$, Mw = 421.50, triclinic, $P\bar{1}$, yellow needle (0.21 × 0.19 × 0.11 mm^3), a = 9.2143(5) Å, b = 12.9784(6) Å, c = 19.545(1) Å, α = 84.112(1)°, β = 77.999(1)°, γ = 78.688(1)°, Z = 4, V = 2237.2(2) Å^3, R1 = 0.0477, 0.0627, wR2 = 0.1304, 0.1450 ($I > 2\sigma(I)$, all data), GOF = 1.031.

Structure of 3b. $C_{39}H_{39}NSiTi$, Mw = 597.70, triclinic, $P\bar{1}$, brown plate (0.05 × 0.15 × 0.30 mm^3), a = 14.282(1) Å, b = 14.388(1) Å, c = 16.505(1) Å, α = 68.603(2)°, β = 82.910(1)°, γ = 81.242(2)°, Z = 4, V = 3112.4(4) Å^3, R1 = 0.0551, 0.1389, wR2 = 0.0808, 0.0946 ($I > 2\sigma(I)$, all data), GOF = 1.031.

Structure of 18. $C_{50}H_{54}K_2O_4$, Mw = 797.13, triclinic, $P\bar{1}$, yellow needle (0.10 × 0.13 × 0.38 mm^3), a = 9.8536(6) Å, b = 12.7084(7) Å, c = 18.994(1) Å, α = 71.511(1)°, β = 89.515(1)°, γ = 77.149(1)°, 173(2) K, Z = 2, V = 2194.2(2) Å^3, R1 = 0.0550, 0.1284, wR2 = 0.1162, 0.1461 ($I > 2\sigma(I)$, all data), GOF = 0.994.

Acknowledgment. We thank Prof. Clark Landis for assistance with magnetization transfer methodology.

Note Added After ASAP Publication. Errors in the figure and table numbering in the Supporting Information were corrected on May 14, 2007.

Supporting Information Available: Polymerization and NMR data used for kinetic models; ethylene−octene polymerization results with **1**, **2**, and **3a**; magnetization transfer NMR data of **16** and its analysis; synthetic procedures for the preparation of **5**−**12** and **15**−**21**; actual NMR spectra of compounds **2**−**22**; comprehensive X-ray data tables for compounds **1**, **2**, **3a**, **3b**, and **18**. This material is available free of charge via the Internet at http://pubs.acs.org.

JA070061Y